Batteries & Supercaps

Research Article
doi.org/10.1002/batt.202300445

Chemistry Europe
European Chemical Societies Publishing

www.batteries-supercaps.org

Thermal Transients to Accelerate Cyclic Aging of Lithium-Ion Batteries

Lisa Cloos,*[a] Oliver Queisser,[a] Ahmed Chahbaz,[b, d] Sabine Paarmann,[a] Dirk Uwe Sauer,[b, c, d, e] and Thomas Wetzel[a]

Cyclic aging tests of lithium-ion batteries are very time-consuming. Therefore, it is necessary to reduce the testing time by tightening the testing conditions. However, the acceleration with this approach is limited without altering the aging mechanisms. In this paper, we investigate whether and how thermal transients accelerate the aging. The tests are performed on NMC/graphite pouch cells by applying temperatures in a range of 5 °C to 45 °C to the cell surface. The results show, that an accelerated capacity loss can be achieved in comparison to the reference cell at a steady-state temperature of 25 °C. However, capacity difference analysis (CDA) prognoses a covering layer for the transient cells, which is confirmed upon post-mortem analysis. We suspect the origin to lie in the dynamics of temperature fields and current distribution during temperature changes when charging. More specifically, areas of higher temperature in the cell lead to high local current densities and plating. Subsequently, high temperatures promote the reaction of the plated lithium with electrolyte. The results show that thermal transients are a critical condition for lifetime and safety and should be treated with caution as they can occur during real life operation.

Introduction

Aging limits the performance of lithium-ion batteries in application.[1] Therefore, tests must be carried out for understanding and reliably predicting the aging effects. Yet, the success already achieved in increasing lifetime of commercial cells creates a burden on attempts to even better understand the aging. The duration of cyclic aging tests under moderate conditions can be immensely time consuming; for example, under moderate temperature conditions (25 °C) cells lasted approximately 4000 equivalent full cycles (EFC) before reaching a remaining capacity of 90% relative to the initial capacity[2] (commonly defined as the State of Health (SoH)). The estimated testing time is more than half a year. Apart from temperature, other stress factors such as the mean state of charge (SoC),[3] depth of discharge (DoD)[4] and mechanical effects[5] are relevant stress-factors on cycle life. Regarding the current rate (C-rate), different consequences for cyclic aging are found. In some cases, the C-rate played a minor role,[6,7] especially when a constant temperature could be ensured via Peltier elements.[6] However, in other contributions increasing the C-rate[7,8] and the temperature level[7,8,9] were used to accelerate cyclic aging tests.

The aging is oftentimes judged by the capacity decrease. Yet, this quantity is no clear indicator for the wide range of underlying, complex and even interacting degradation mechanisms. However, those mechanisms need to be understood in order to accelerate the aging. On the other hand, the acceleration of cyclic aging tests should not trigger degradation mechanisms different from those of the reference tests.[10]

Looking at the aging mechanisms triggered by different temperature levels, two main mechanisms are separated by the optimum temperature, that lies in the region around 25 °C.[11–13] Below that optimum temperature, lithium plating is mostly the dominant aging mechanism, whereas at higher temperatures, solid electrolyte interface (SEI) layer thickness increases due to electrolyte decomposition.[11] Increasing the temperature beyond 45 °C leads to further changes. Zhang et al.[14] found a negative impact on the capacity fade for an SEI forming temperature higher than 45 °C. Ramadass et al.[15] observed repeated film formation, which led to an increased lithium loss

[a] L. Cloos, O. Queisser, Dr.-Ing. S. Paarmann, Prof. Dr.-Ing. T. Wetzel
Institute of Thermal Process Engineering (TVT)
Karlsruhe Institute of Technology (KIT)
Kaiserstraße 12, 76131 Karlsruhe, Germany
E-mail: lisa.cloos@kit.edu

[b] A. Chahbaz, Prof. Dr. rer. nat. D. U. Sauer
Chair for Electrochemical Energy Conversion and Storage Systems, Institute for Power Electronics and Electrical Drives (ISEA)
RWTH Aachen University
Campus-Boulevard 89, 52074 Aachen, Germany

[c] Prof. Dr. rer. nat. D. U. Sauer
Institute for Power Generation and Storage Systems (PGS), E.ON ERC
RWTH Aachen University
Mathieustrasse 10, 52074 Aachen, Germany

[d] A. Chahbaz, Prof. Dr. rer. nat. D. U. Sauer
Jülich Aachen Research Alliance
JARA-Energy
Templergraben 55, 52056 Aachen, Germany

[e] Prof. Dr. rer. nat. D. U. Sauer
Helmholtz Institute Münster (HI MS), IEK 12
Forschungszentrum Jülich
52425 Jülich, Germany

and increase in anode resistance.[15] Clearly, acceleration of cyclic aging by temperature increase is limited by the change in aging mechanisms, as these change at high temperature levels. However, there are findings in literature suggesting that thermal transients are an additional factor to accelerate aging. Werner et al.[12] have seen a significantly increased capacity loss for cells, that cycled while constantly changing the temperature between 0 °C and 50 °C. Both Paarmann et al.[16] and Carter et al.[17] detected lithium plating for cells subjected to a temperature change.

Additionally, the temperature of a cell after lithium plating already occurred seems to be a decisive factor for the further aging, as it impacts the reaction rate of the plated lithium with electrolyte. Plated lithium from low temperature cycling can react with the electrolyte to insoluble and hardly conductive products.[18] SEI formation is mostly accompanied with gas evolution.[19] If gassing due to the reaction of electrolyte with plated lithium occurred, this gassing is intensified by storing that cell at a higher temperature of 40 °C.[20] Chang et al.[21] did not only increase the ambient temperature from 10 °C to 60 °C, but kept on cycling, which led to rapid failure of the cells. This cell failure was also induced by the reaction of lithium-rich SEI with electrolyte, which led to severe gassing.[21] The change to a higher temperature is also suspected to be of importance by Paarmann et al.[16] They suggested, that increasing the temperature from 0 °C to 50 °C during charging influences the reaction rates of all occurring processes slightly different enabling lithium plating.[16]

These findings clearly show that temperature changes with certain combinations of higher and lower temperatures during cycling can accelerate the capacity loss. Generally, different charging and discharging temperatures affect the capacity loss even with thermal equilibration between charging and discharging steps.[22] Ruiz et al.[22] found a linear dependency between capacity loss and discharging temperature and a quadratic relation for the charging temperature. This accentuates the importance of the temperature during charging. The charging temperature can induce lithium plating and the following temperature can facilitate further reactions.[20,21] In this work, we intend to explore the effects of superimposed temperature changes during cycling in detail with the focus on their ability to accelerate cyclic aging. Therefore, we need to understand the occurring aging mechanisms as they should not differ from the aging mechanisms of the reference case at homogeneous steady-state temperature. With this background, we avoid high temperatures, such as 60 °C to exclude unwanted effects leading to sudden cell failure. To trigger accelerated aging nonetheless, we choose several temperature boundary conditions in the range of 5 °C to 45 °C. These temperature boundary conditions are applied to the surface of the cells via cooling plates. Special emphasis is put on the temperatures during charging, as they seem particularly relevant.[22] Therefore, the temperature changes have been set synchronous to the electric cycles, i.e. they always occur at the beginning of each charge and discharge step. Meanwhile, the C-rate is kept constant at C/2 in charge and 1 C in discharge direction. The synchronization leads to the same predominant temperature over the entire aging course during each charging (*ch*) and discharging (*dch*) step respectively (more details in "Experimental Section"). With these experiments we intend to understand what aging mechanisms are triggered by thermal transients. This is used to evaluate thermal transients as a way to accelerate cyclic aging in comparison to reference conditions at a steady-state temperature.

Results and Discussion

The potential of the investigated temperature changes to accelerate cyclic aging is judged by the remaining capacity (SoH) in comparison to the reference cases at a homogeneous steady-state temperature. These are 5 °C, 25 °C and 45 °C with the main focus on the reference case at 25 °C. Minimum aging is expected for this optimum temperature region,[11–13] which is favorable in application, for example in battery electric vehicles.[13] In the following, the predominant aging mechanisms are evaluated with non-invasive methods and then confirmed with post-mortem analysis. Pulse resistance, capacity difference analysis (CDA)[23] and Differential Voltage Analysis (DVA)[24] are used as first indicators for the occurring dominant aging mechanisms.

Capacity and Resistance

The relative nominal capacity decrease over EFC, which is the charge throughput of one full cycle divided by the charge throughput of one full cycle at Beginning of Life (BoL) at nominal conditions is shown in Figure 1(a). The upper image shows the results for all investigated boundary conditions, while the lower two images provide zooms in different regions. Cells, that were cycled at steady-state temperature conditions, are marked with circles. These are the reference conditions for the cells, that experienced temperature transients during cycling (*T*), which are indicated with stars. The colors represent the equivalent aging temperature[12] (blue 5 °C, turquoise 15 °C, green 25 °C, orange 35 °C and red 45 °C), which is a spatial and temporal mean value for the dynamic and inhomogeneous temperature boundary condition. The actual surface temperatures during electrical load are given in Table 2 (Experimental Section). Two main groups can be differentiated at first sight. All cells that were charged at 5 °C experience a drastic capacity decrease (5 $^{\circ}C$, T 25 $^{\circ}C_{dch}$ 5 $^{\circ}C_{ch}$ and T 45 $^{\circ}C_{dch}$ 5 $^{\circ}C_{ch}$; in the following: group A). This is true for all cells no matter if they were exposed to a temperature transient or not. Still, the cells cycled under transient conditions (T 25 $^{\circ}C_{dch}$ 5 $^{\circ}C_{ch}$ and T 45 $^{\circ}C_{dch}$ 5 $^{\circ}C_{ch}$) reached even lower SoHs than the cells at a steady-state temperature of 5 °C. Whereas both cells at T 45 $^{\circ}C_{dch}$ 5 $^{\circ}C_{ch}$ experienced an equally steep capacity decrease, the capacity decrease of the cells at T 25 $^{\circ}C_{dch}$ 5 $^{\circ}C_{ch}$ differ strongly from each other. Noticeably, variance is high for this group A.

All other cells remained at a relative capacity above 90 % after ~600 EFC (in the following: group B). The highest capacity

Research Article
doi.org/10.1002/batt.202300445
Chemistry Europe
European Chemical Societies Publishing

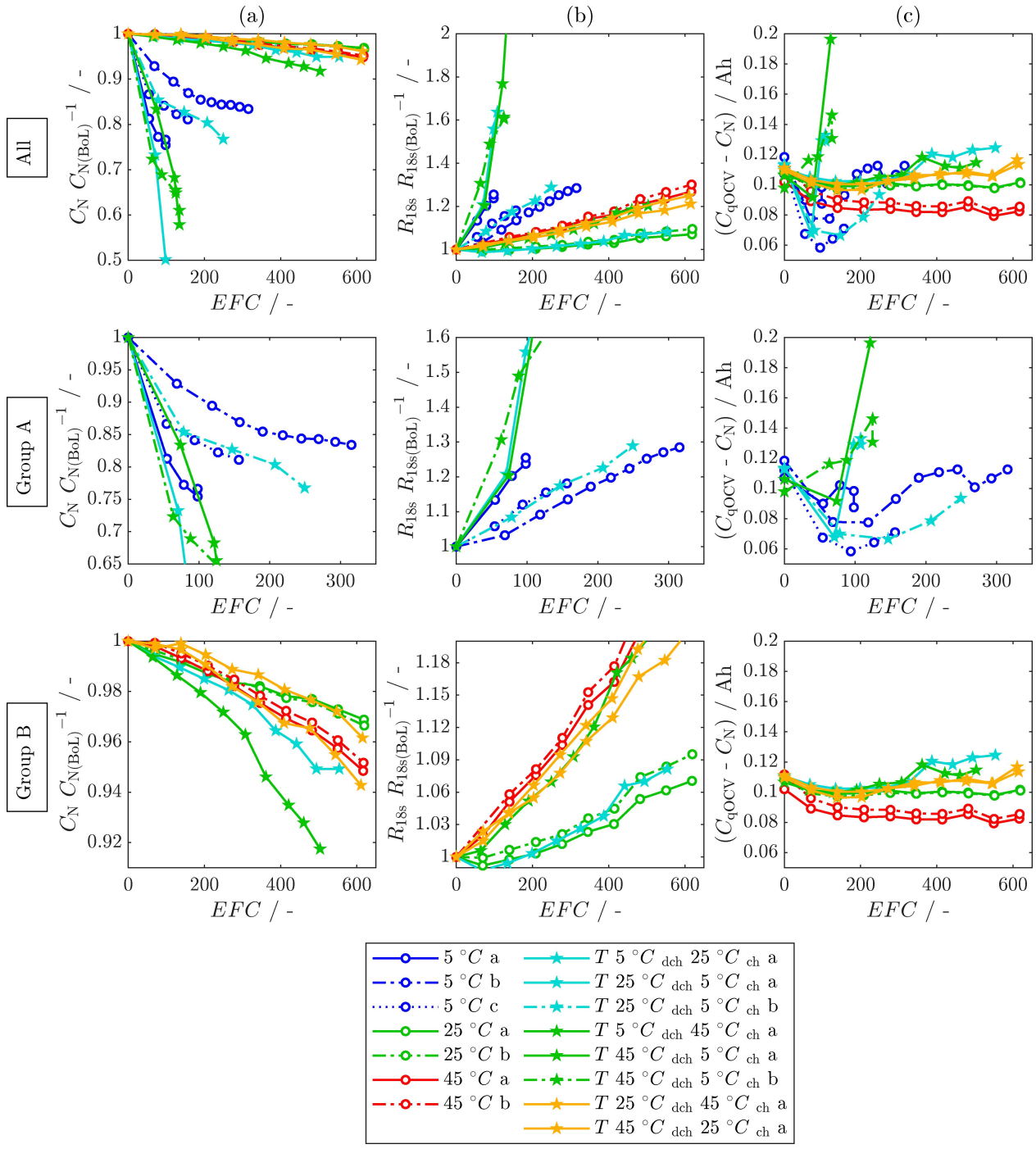

Figure 1. (a) Relative nominal capacity decrease over EFC; (b) Relative pulse resistance increase over EFC; (c) Capacity difference of quasi-OCV and nominal capacity over EFC of all cells, zoom of Group A and zoom of Group B.

after more than 600 EFC was achieved for the cells aged at steady-state temperature of 25 °C. The steady-state cells at 45 °C experienced a slightly steeper capacity decrease. The cells that were cycled between 25 °C and 45 °C followed the trend of their steady-state counterpart according to their charging temperature (T 25 °C_{dch} 45 °C_{ch} and 45 °C; T 45 °C_{dch} 25 °C_{ch} and 25 °C). The trajectory was only slightly steeper for the transient cells. This correlation does not apply to the transient cells, that were discharged at 5 °C (T 5 °C_{dch} 45 °C_{ch} and T 5 °C_{dch} 25 °C_{ch}). They had a steeper capacity decrease than their steady-state counterparts at the respective charging temperature. Thereby, the capacity decrease was more severe for the cell with the larger temperature difference (T 5 °C_{dch} 45 °C_{ch}). The cells in group A all had approximately a linear capacity decrease. The difference in capacity decrease for the steady-state cells (25 °C and 45 °C) was low respectively. The difference of the two cells at 25 °C amounted to 0.2 % SoH at the last reference performance test (RPT) after 600 EFC.

Research Article
doi.org/10.1002/batt.202300445
Chemistry Europe
European Chemical Societies Publishing

The cells cycled at a steady-state temperature (5 °C, 25 °C and 45 °C) followed the expected aging trend according to literature with the minimal aging at the optimum temperature around 25 °C and increased capacity loss for higher (45 °C) and lower (5 °C) temperatures.[11] Even so, there was a steep capacity decrease and no reproducibility for cells cycled at 5 °C or more generally group A. Therefore, the results of group A are not reliable and we can conclude that a charging temperature of 5 °C in combination with a charging C-rate of C/2 is abusive for this high-energy cell. The aging mechanisms leading to this failure will be discussed in due course.

The cells, that were discharged at 5 °C and charged at a higher temperature (T 5 °C$_{dch}$ 45 °C$_{ch}$ and T 5 °C$_{dch}$ 25 °C$_{ch}$) still experienced a faster capacity decrease than all other cells of group B but not as drastically as group A. Notably, T 5 °C$_{dch}$ 45 °C$_{ch}$ aged even faster than the reference counterpart at the highest occurring temperature of 45 °C. In comparison to the cell aged at the steady-state reference temperature of 25 °C the transient cell lost the capacity approximately three times faster (linear relative nominal capacity decrease per EFC).

The question to discuss is why group A experienced a steep capacity decrease and if the aging mechanisms within the cells of group B are comparable between the steady-state and transient cells. To start getting an idea of the root cause, the pulse resistance and the CDA are evaluated. The pulse resistance increase is plotted in Figure 1(b). The two cell groups are visible again in the upper plot. The lower two plots zoom into both groups respectively. A steeper pulse resistance increase can be seen for the cells at group A. This time, group B can be divided in two subgroups. The cells with an equivalent aging temperature of 25 °C and lower (25 °C, T 5 °C$_{dch}$ 25 °C$_{ch}$) experienced a slower resistance increase than the cells at a higher equivalent aging temperature. The same cells also had a decrease in resistance in the first EFCs, before it started to increase.

A resistance decrease for a steady-state aging temperature of 25 °C over the first cycles has been seen before[12,25] and could indicate a decrease in SEI resistance due to an easier desolvation of Li^+ ions of the still forming SEI.[26] A resistance increase on the other hand was correlated both to the anode thickness increase due to SEI build up[11] as well as to an increase in surface resistance of the cathode due to oxidation.[27] Especially, the first one explains the resistance increase of the cells with a higher equivalent aging temperature in group B. It does not explain the resistance increase of group A. Therefore, CDA will be examined.

The CDA, which is the capacity difference of different C-rates, is a way to measure the lateral diffusion of lithium ions in the anode.[23] An increase in CDA indicates the formation of a covering layer or an inhomogeneous lithium distribution.[28] Here, we used the difference in capacity between discharging with C/15, which is the chosen C-rate for the quasi-Open Circuit Voltage (OCV), and nominal C-rate C/3 that were part of the RPT routine at 25 °C (Figure 1(c)). An increase of this difference over aging can be seen for group A and all transient cells especially for the cells at higher temperatures between 25 °C and 45 °C (T 25 °C$_{dch}$ 45 °C$_{ch}$ and T 45 °C$_{dch}$ 25 °C$_{ch}$).

Due to these results, we suspect the formation of a covering layer for group A, which then led to a steep increase in resistance. A potential covering layer formation for all other transient conditions is unexpected, as they did not have a much steeper capacity decrease than the steady-state conditions. Additionally, a covering layer formation for the cells at higher temperatures between 25 °C and 45 °C (T 25 °C$_{dch}$ 45 °C$_{ch}$ and T 45 °C$_{dch}$ 25 °C$_{ch}$) is uncommon as plating is expected for lower temperatures.[11] This increase of capacity difference for the transient cells of group B occurred at around EFC 300, which was found after a similar number of EFC for the cells of Willenberg et al.[29] They similarly suspected the onset of a covering layer formation which was confirmed during post-mortem analysis.

So far, we have discovered, that 5 °C charging temperature is abusive for the investigated cell. A steep pulse resistance increase and CDA points towards potential cover layer build-up. Nevertheless, a thermal transient condition with 5 °C discharging and 45 °C charging temperature (T 5 °C$_{dch}$ 45 °C$_{ch}$) is a promising aging acceleration condition as the investigated cell ages 3 times faster than the reference cells at 25 °C. Still, the dominant aging mechanisms in both conditions needs to be evaluated. Next, results of DVA and their utilization to identify main degradation modes will be presented.

Differential Voltage Analysis

The DVA was performed for both the steady-state reference and selected transient conditions. But first, balancing of anode and cathode half-cell measurements[24] was done to assign the occurring degradation modes to each electrode (Figure 2). The graphite DVA curve peaks are all visible in the full cell DVA. The cathode DVA does not have any peaks and can best be evaluated by the steep differential voltage increase on the right (C), which limits the full cell capacity.

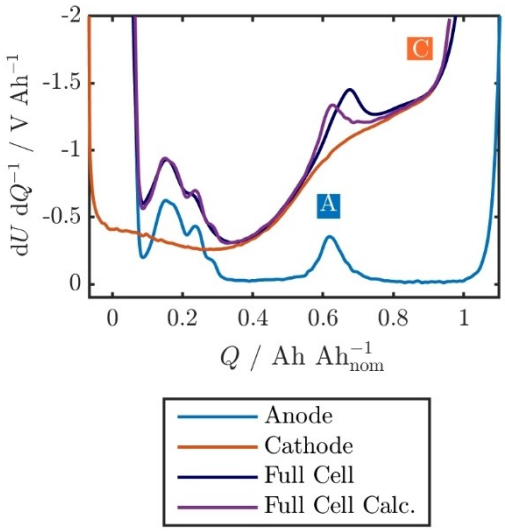

Figure 2. Balancing of anode and cathode DVA to full cell DVA. (Blue: anode; orange: cathode).

Research Article
doi.org/10.1002/batt.202300445
Chemistry Europe
European Chemical Societies Publishing

The pouch cell DVAs are evaluated for all RPT and the respective SoH is indicated by the color-code in Figure 3. The cell aged at a steady-state temperature of 45 °C still shows very sharp anode peaks. Only the cathode curve (C) is shifted to the left. This shift to the left is also seen less pronounced for the cell aged at a steady-state temperature of 25 °C. Here, the anode peak (A) flattened additionally. The shift of the cathode curve (C) is most severe for the cell aged at 5 °C. In this case the anode peak (A) cannot be precisely located.

In the bottom row of Figure 3, DVA curves of three transient cells are shown. Not only the most promising aging acceleration condition (T 5 °C_{dch} 45 °C_{ch}) is evaluated, but also the two transient cells with a higher mean temperature than 25 °C (T 25 °C_{dch} 45 °C_{ch} and T 45 °C_{dch} 25 °C_{ch}), whose increase in CDA was surprising considering their mild capacity decrease. Additionally, they were not exposed to a 5 °C environment, which means that any abusive charging condition can be ruled out. All represented cells show a shift of the cathode curve (C) to the left – the extent varying proportionally to the capacity decrease – and a flattening of anode peak (A). The cell T 5 °C_{dch} 45 °C_{ch} shows a slight shift of peak A to the left, whereas the DVA of the transient cell T 45 °C_{dch} 25 °C_{ch} is almost indistinguishable to that of the cell at 25 °C. The cathode curve (C) moves to the left for all shown DVAs. The slope (C) does not increase considerably, which means there is no severe contraction indicating Loss of Active Material (LAM) on the cathode.[24] In this case, thermal transients do not have a crucial effect on the cathode for the investigated cell. However, the cathode curve shifts to the left due to parasitic side reactions,[24] in short Loss of Lithium Inventory (LLI).[30] The main degradation mode of this NMC532-graphite cell seems to be LLI, which was also seen for a similar cell by Gilbert et al.[31] The flattening of the anode peak (A) is obvious for all cells except the higher steady-state temperature (45 °C). The flattening can be due to an inhomogeneous lithium distribution,[32] that can be caused by an impermeable covering layer from passivated lithium ions as result of prior plating.[33] The impermeable cover layer also induces LAM on the anode.[32,34] However, the shrinkage of the anode curve indicating LAM on the anode[24] can only be seen for the transient condition T 5 °C_{dch} 45 °C_{ch}, which already reached lower SoH, to a minimum extent.

In summary, LLI is recognized as the main degradation mode for the presented cell. DVA revealed no major differences of the changes in DVA between the steady-state and transient conditions in group B. Interestingly, the DVA of the T 45 °C_{dch} 25 °C_{ch} and 25 °C cells are almost indistinguishable. Only a slight shift of the anode peak could be seen for the transient potential aging acceleration condition (T 5 °C_{dch} 45 °C_{ch}). Nevertheless, additional indicators are necessary to compare dominant aging mechanisms. A cell-opening has therefore been conducted to explain previous findings from CDA and DVA.

Post-mortem Analysis

Post-mortem analysis is used to support previous hypotheses about potential covering layer formation. Therefore, this analysis consists of a visual inspection of the anode, cathode and separator after cell-opening. Already before cell-opening, visible gassing was noticed for the condition T 45 °C_{dch} 5 °C_{ch}, at which both reproduction cells experienced a steep capacity decrease. This indicates a reaction of electrolyte with lithium rich-SEI in line with the results by Chang et al.,[21] who observed gas generation during cycling after transitioning from 0 °C to temperatures above 20 °C.

The same cells as discussed in the DVA and the gassed cell (T 45 °C_{dch} 5 °C_{ch} *b*) were opened in an inert argon atmosphere. No cathodes showed visible signs of degradation upon inspection. An excerpt of the anode at the center of the jelly

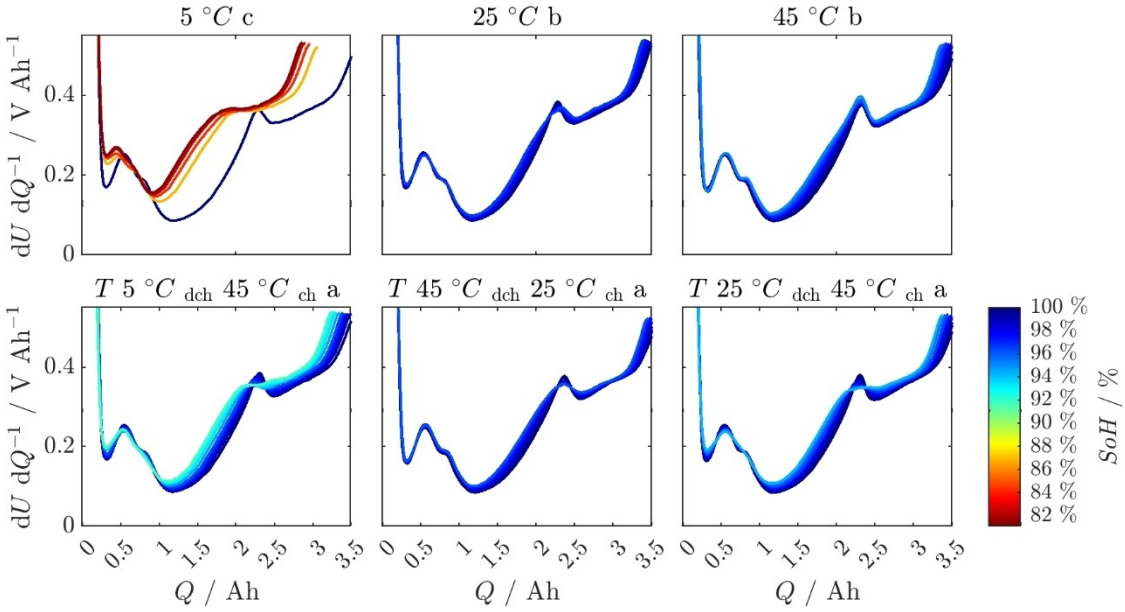

Figure 3. DVA in charge direction over SoH for the steady-state cells (5 °C *c*, 25 °C *b* and 45 °C *b*), the potential aging acceleration condition (T 5 °C_{dch} 45 °C_{ch} *a*) and the transient cells T 45 °C_{dch} 25 °C_{ch} *a* and T 25 °C_{dch} 45 °C_{ch} *a* with an equivalent aging temperature higher than 25 °C.

Research Article
doi.org/10.1002/batt.202300445
Chemistry Europe
European Chemical Societies Publishing

roll for each opened cell is shown in Figure 4. Due to the winding of the anode, bends in the sheets and delamination of anode active material could be seen. In the following the area between the bends is referred to as a "sheet".

The anode of the cell cycled at 5 °C had an allover metallic covering layer, which was most obvious towards the edges. In the center of the sheets small amounts of the covering layer pulled off and stuck to the separator. In contrast, the cells at a higher steady-state temperature did not show any depositions. However, a color difference could be seen between 25 °*C* and 45 °*C*. The cell at the higher steady-state temperature (45 °*C*) had a lighter blueish coloration on the inner layers of the jelly-roll and a darker blue coloration on the outer layers. The anode sheets of cell 25 °*C* were generally black with only a blueish tint on the inner layers of the jelly-roll. It must be noted, that the interpretation of color needs to be handled with caution as it is strongly impacted by external factors. Another clue could be gathered during cell disassembly. The sheets of cell 45 °*C* were drier than the sheets of cell 25 °*C*.

At first sight, depositions were visible for all opened transient cells, even the ones at equivalent aging temperatures above 25 °C. The most severe covering layer was found for the transient cell of group A (*T* 45 °C_{dch} 5 °C_{ch}). Here, the metallic sheen in the bends and the delamination of the covering layer was even more pronounced than for the steady-state cell at 5 °C. The other transient cells shown in Figure 4 formed localized covering layers. Opposite to these depositions, the separator had a yellowish tint. The depositions themselves varied in location, distribution and color between the different temperature conditions. The depositions of the transient cells appeared generally less metallic. However, some parts were reflective under certain light conditions. The location of the covering layer was similar for the cells charged at 45 °C (*T* 5 °C_{dch} 45 °C_{ch} and *T* 25 °C_{dch} 45 °C_{ch}). They both showed the most severe deposition in the center of the jelly roll in the middle of the sheet. Whereas the *T* 25 °C_{dch} 45 °C_{ch} only had depositions in the very center of the jelly roll, the depositions of cell *T* 5 °C_{dch} 45 °C_{ch} appeared throughout the whole jelly roll. On the other hand, *T* 45 °C_{dch} 25 °C_{ch} showed depositions in the bends of the jelly roll and on the opposite side of the current collectors. In the picture shown in Figure 4 the deposition spread towards the middle of the sheet. Next to the covering layers, the cells with a higher equivalent aging temperature than 25 °C had a similar coloration throughout the whole jelly-roll like their reference counterparts at the respective charging temperature. The different colorations of the anode sheets and all-over and partial covering layers need to be put into context and discussed with previous results.

Discussion

Solely from the analysis of the capacity decrease, we have found a suitable accelerated aging condition in the transient condition of a 5 °C discharging and 45 °C charging temperature (*T* 5 °C_{dch} 45 °C_{ch}) compared to the steady-state reference condition at 25 °C and even 45 °C. However, it still needs to be discussed, whether it mirrors the aging mechanisms of the reference conditions. CDA predicted a covering layer formation for the cells cycled with superimposed temperature changes, which was confirmed by post-mortem analysis and was not found for the steady-state reference cells. Interestingly, temperature changes with equivalent aging temperature above 25 °C also led to some covering layer formation. A summary of the results so far is given in Table 1. Thereby, the arrows indicate the qualitative change of the variable. They vary from strong decrease (↓↓) over no clear change distinguishable (→) to strong increase (↑↑).

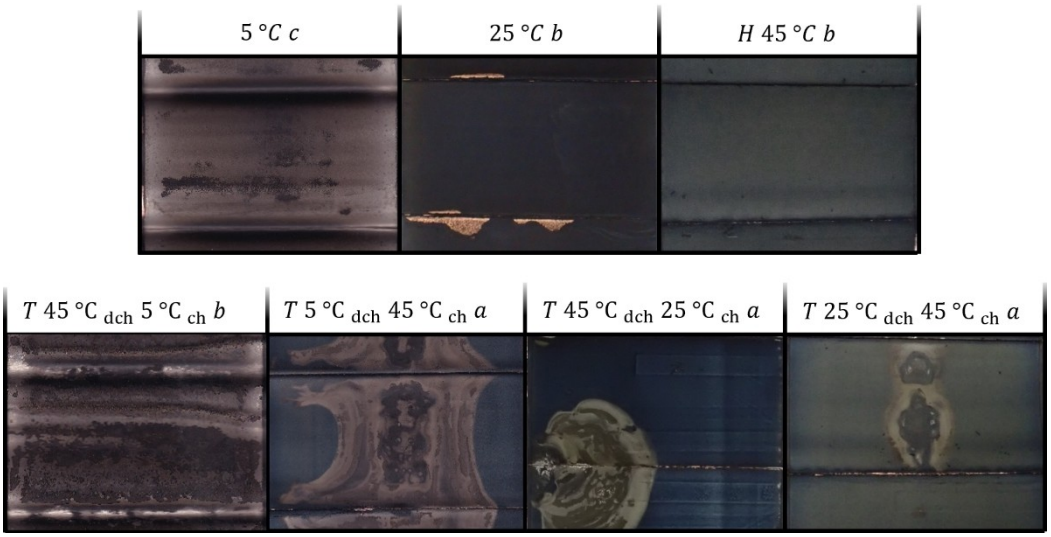

Figure 4. Anodes close to the center of the jelly roll of reference conditions (5 °*C c*, 25 °*C b* and 45 °*C b*), of the cell with very steep capacity decrease (*T* 45 °C_{dch} 5 °C_{ch} *b*), of the potential aging acceleration condition (*T* 5 °C_{dch} 45 °C_{ch} *a*) and of the transient cells *T* 45 °C_{dch} 25 °C_{ch} *a* and *T* 25 °C_{dch} 45 °C_{ch} *a* with an equivalent aging temperature higher than 25 °C.

Research Article
doi.org/10.1002/batt.202300445
Chemistry Europe
European Chemical Societies Publishing

Table 1. Overview over cells and respective investigations (Arrows qualitatively describe the change of the value in comparison to BoL, ↑↑ strong increase, ↑ mild increase, → no clear change visible, ↓ mild decrease, ↓↓ strong decrease).

Cell name	*T* condition	C_N $C_{N(BoL)}^{-1}$	R_{Pol} $R_{Pol(BoL)}^{-1}$	CDA	DVA	Visual Inspection
5 °C *a*	steady-state 5 °C	↓↓	↑↑	↑↑		
5 °C *b*		↓↓	↑↑	↑↑		
5 °C *c*		↓↓	↑↑	↑↑	LLI ↑↑ Anode peak flat	Metallic cover layer
25 °C *a*	steady-state 25 °C	→	→	→		
25 °C *b*		→	→	→	LLI ↑ Anode peak flat	Black to dark blue color
45 °C *a*	steady-state 45 °C	→	↑	→		
45 °C *b*		→	↑	→	LLI ↑	Dark blue to light blue color
T* 5 °C$_{dch}$ 25 °C$_{ch}$ *a	transient 5 °C discharge 25 °C charge	↓	→	↑		
T* 25 °C$_{dch}$ 5 °C$_{ch}$ *a	transient 25 °C discharge 5 °C charge	↓↓	↑↑	↑↑		
T* 25 °C$_{dch}$ 5 °C$_{ch}$ *b		↓↓	↑↑	↑↑		
T* 5 °C$_{dch}$ 45 °C$_{ch}$ *a	transient 5 °C discharge 45 °C charge	↓	↑	↑	LLI ↑ LAM Anode ↑ Anode peak flat	Cover layer in the center of the sheets throughout the whole jelly-roll
T* 45 °C$_{dch}$ 5 °C$_{ch}$ *a	transient 45 °C discharge 5 °C charge	↓↓	↑↑	↑↑		
T* 45 °C$_{dch}$ 5 °C$_{ch}$ *b		↓↓	↑↑	↑↑		Metallic cover layer, delamination of cover layer
T* 25 °C$_{dch}$ 45 °C$_{ch}$ *a	transient 25 °C discharge 45 °C charge	→	↑	↑	LLI ↑ Anode peak flat	Cover layer in the center of the sheets only in the center of the jelly roll
T* 45 °C$_{dch}$ 25 °C$_{ch}$ *a	transient 45 °C discharge 25 °C charge	→	↑	↑	LLI ↑ Anode peak flat	Cover layer in the bends and opposite to the tabs

Aging Mechanisms of Reference Conditions

Due to the metallic depositions of the cell cycled at the low temperature (5 °C) we suspect lithium plating, which is a common aging mechanism at low temperatures.[11,35] The same conclusion was drawn by Burns et al.,[36] who saw a very similar covering layer for higher C-rates for a similar cell format. The higher amount of metallic sheen on the edges of the jelly roll can be explained by the edge effect, where plating is preferred due to higher overpotentials within this area.[37] Overlithiating the edge of the cathode opposite the anode overhang during discharging leads to inhomogeneities and plating on the anode while charging.[38]

For higher temperatures (45 °C), we noticed different coloration of the anode sheets and dryness of the electrode sheets in comparison to the nominal condition at 25 °C. LiC_{18} phase is blue in color,[39] which means incomplete delithiation. The dryness of the electrode sheets of cell 45 °C points towards electrolyte decomposition and increased SEI formation.[34] At higher temperatures, reaction rates increase and SEI growth becomes dominant.[11] As a result, active lithium is consumed (LLI), which explains the decreased capacity of the steady-state condition at 45 °C in comparison to steady-state condition at 25 °C.

Aging Mechanisms of Transient Conditions

Starting with the transient cells at a higher equivalent aging temperature than 25 °C, a similar coloration of the anode sheets was seen compared to the reference counterparts at the respective charging temperature. Similarly, the capacity loss was only slightly steeper for the transient cells. We consider increased SEI formation at the higher charging temperature as a reason for the capacity decrease at the transient condition. The formation of covering layers in certain areas of the transient cells, which can passivate active material of the anode,[32,34] did not seem to be detrimental for the capacity fade yet. This process would only become dominant, if LAM of the anode, which is usually oversized, becomes dominant.[40] Attia et al.[40] described this phenomenon as a typical hidden knee. The flattening of the anode peak (A) in the DVAs might be an

additional indicator of a lithium distribution inhomogeneity, possibly due to a passivated lithium covering layer.[33] However, slight flattening of the anode peak (A) was also visible for the reference condition at 25 °C. Since no covering layer was visible for this condition, this might have solely been due to lithium distribution inhomogeneity.

To unravel the reason for the observed covering layers, the location, distribution and color are discussed in more detail. The covering layers of the transient cells are not only more inhomogeneous but also less metallic in some areas compared to the covering layer of the reference cell at low temperature (5 °C). This could indicate that the deposited metallic lithium has already reacted with electrolyte.[18] This process is facilitated for the transient cells, since the reaction can take place during the time at a higher temperature.[20,21] This process has the most extreme effect for the transients including a 5 °C charging and 45 °C discharging (T 45 °C_{dch} 5 °C_{ch}), which leads to an even more pronounced capacity decrease than for the steady-state reference condition at 5 °C. An additional consequence was the strong delamination of covering layer and/or active material.

The depositions found on the anodes of the opened transient cells showed similar positions according to the sequence of the temperature change during charging. The cells, that were originally at a lower temperature and changed to a higher temperature at the beginning of charge, showed the strongest depositions in the center of the jelly roll, in the center of the sheet. This is exactly where cells are known to increase in temperature due the interplay of heat generation and limited conduction.[41] Especially, if the temperature is low, the heat generation will be high due to higher irreversible losses caused by increased resistances.[42]

Further, the cell that started charging at a higher temperature and changed to a lower one, showed depositions mostly in the bends of the jelly roll and at the electrode edge opposing the tabs. There, they almost seem to have grown from an initial plating spot. This is possible, because lithium plating is a heterogeneous nucleation process.[43] In the bends mechanical effects might play a role. However, the windings are the same for all cells, and the temperature was varied. Therefore, we attribute difference in covering layer formation to the temperature boundary conditions. For both conditions the temperature field during the temperature change should be looked at in more detail.

Two effects are at play here, which are heat source and heat conduction from the cell to the thermal plates, which will affect the top and bottom surface of the pouch cell in contact with the thermal plates first. This means, that during the cool down of the cell (Figure 5a), the sides of the cells, that are not touching the cooling plates, will probably remain at the higher temperature for a slightly longer time due to longer heat transport pathways. Secondly, heat generation will have an impact, which will increase the temperature in the center of the cell as already described above. The heat generation will have a greater effect for a cell at lower temperature level due to increased resistances.[44] In the case, where the cell has a lower temperature than the thermal plates at the beginning of charge (Figure 5b), the center and the sides touching the plates will

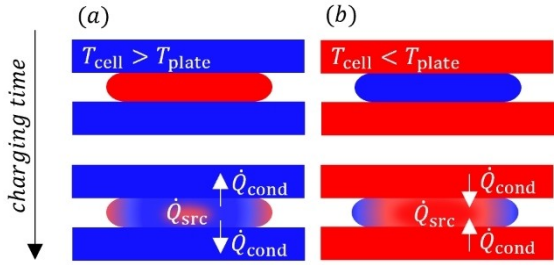

Figure 5. Schematic illustration of the temperature field during the temperature change for two scenarios; cell has a higher (red) (a) or lower (blue) (b) temperature than the cooling plate.

increase in temperature faster due to both effects simultaneously. An schematic illustration of the temperature fields described is given in Figure 5.

Taking into account, that the different sequences of temperature change led to different temperature fields inside the cell during beginning of charge, the effect of this temperature field should be evaluated. Temperature, resistance and current are strongly interlinked.[45] Therefore, we suppose, that in the regions of higher temperature, the current densities are higher, which can lead to lithium deposition. A similar reason was found for steady-state inhomogeneous temperature conditions which led to an inhomogeneous lithium distribution,[46,47] disturbed the electrode balancing and locally violated the lithium plating condition.[47] Metallic lithium deposits if the anode potential falls below 0 V.[35] A further consequence could be local overcharge of the anode due to the higher current densities.[33] A hint for this theory represent the yellow stains on the separator, which were found as a sign of overcharge by Chang et al.[21]

This also answers the question whether the abusive charging condition of 5 °C, that is still present for a short amount of time in the beginning of charging is the reason for the larger capacity fade of the T 5 °C_{dch} 45 °C_{ch} a cell in comparison to the reference cell at 25 °C. The covering layer formation of the transient cell occurred in the warmer regions during the temperature change at the beginning of charge and is therefore only indirectly related to the presence of the low temperature. Also, the presence of a temperature above 25 °C could lead to enhanced passivation,[20,21] which can explain the increased capacity loss for cell T 5 °C_{dch} 45 °C_{ch} a in comparison to T 5 °C_{dch} 25 °C_{ch} a. This is in line with the findings from Werner et al.[2,12] In the same study,[2,12] plating did not occur in the regions of higher temperature, but in the regions of 0 °C for an inhomogeneous steady-state temperature condition.[16] However, one has to note that the cell under investigation was a high power cell,[2] which is not as sensitive to high currents. As summarized by Waldmann et al.,[48] plating happens during cycling due to a combination of low temperature, high current or high SoC. In the study of Werner et al.[2,12] and Paarmann et al.,[16] the low temperature presumably was decisive. Their findings in combination with this work also explain, why thermal transients – including a high temperature – lead to a stronger capacity decrease in comparison to steady-state

inhomogeneous temperature fields.[12] When plating happens due to the lower temperature, only in the transient condition this plating will be exposed to a higher temperature and can react more easily.[20,21] This is again in line with the finding, that thermal transient between 0 °C and 25 °C led to less severe aging.[12]

Further insights could be gathered on electrode level. Fear et al.[49] have already shown with a physics informed model, that interelectrode steady-state thermal gradients can shift the potential of the electrodes, which can lead to lithium plating. We suspect the behavior to be even more complex for temperature changes. Rate-determining processes could change upon temperature change.[16]

Potential of Thermal Transients for Aging Acceleration

Now, that the main aging mechanisms of the transient conditions were discussed, their potential to accelerate aging mechanisms of the reference conditions needs to be evaluated. Therefore, the dominant aging mechanisms at the reference conditions are summarized. We suggest LLI to be the main degradation mode for all reference temperature levels. At low temperatures (5 °C) homogeneous lithium plating would be the main aging mechanism causing LLI. Potential LAM of the anode could not be verified due to the disappearance of anode peaks in DVA. At higher temperatures (45 °C) we have identified increased SEI growth in comparison to 25 °C to cause LLI. At moderate temperatures (25 °C) we also suggest the presence of lithium distribution inhomogeneity.

Increasing the temperature to 45 °C after plating at low temperatures enabled reaction of the plated lithium.[20,21] Even lower SoHs were reached for this transient condition (T 45 °C$_{dch}$ 5 °C$_{ch}$) compared to the reference condition at 5 °C. Even though, lithium plating was also occurring, further reaction with electrolyte led to gassing, which is not comparable to the reference condition at 5 °C. This means, that the transients in group A cannot be considered an appropriate acceleration condition for the reference conditions at 5 °C let alone at 25 °C.

Transient conditions, that did not involve a 5 °C charging temperature, still showed local cover layer formation, which was already predicted by CDA. In the case of higher equivalent aging temperature, these covering layers were not dominant, hence, could not be seen in the capacity fade yet. We suggest, that lithium depositions resulted from high current densities due to temperature inhomogeneities during the temperature change at the beginning of charge. The capacity fade was comparable to that of the respective reference charging condition. No acceleration could be achieved.

Just looking at the capacity loss, aging acceleration with thermal transients for the transient condition between 5 °C discharging and 45 °C charging (T 5 °C$_{dch}$ 45 °C$_{ch}$) was possible. This condition experienced an approximately three times increased relative capacity fade in comparison to the steady-state condition at 25 °C. The capacity fade was even increased compared to the reference condition at 45 °C. However, DVA, CDA and post-mortem analysis suggested an additional degradation mode on top of LLI, being LAM of the anode. More specifically, a covering layer on the anode most likely led to inactivation of anode active material.[32,34] Therefore, transferability to steady-state conditions is not given.

We can conclude, that thermal transients do not accelerate the reference testing conditions, but potentially accelerate real-life aging scenarios. Both in automotive real-life driving cycles[13] and during fast-charging,[50] temperatures can increase considerably. However, the temperature changes in these applications are delayed in comparison to the performed experiments. Additionally, the investigated temperature changes were comparably large with up to 40 K. But also smaller temperature differences of 10 K showed lithium depositions in the investigation of Carter et al.[17] Furthermore, they demonstrated, that the deposited lithium can cause catastrophic failure and lead to a lower temperature onset for thermal runaway.[17]

Conclusions

In this paper, we investigated the potential acceleration of cyclic aging with superimposed temperature changes. Therefore, we chose temperatures in the range of 5 °C to 45 °C intending not to trigger different aging mechanisms at even higher temperatures. The capacity loss could be accelerated, however CDA prognosed a cover layer formation for all transient cells, which was confirmed upon cell opening. DVA could not predict this reliably. The location of the formed cover layers of the transient cells could be correlated to the temperature field during the temperature change at beginning of charge. We assume, that like in cells with a steady-state inhomogeneous temperature field, the areas with the higher temperature experience a higher current density, inducing lithium plating.[46,47] Another influence might be locally changing kinetics due to changing temperatures.[16] Additionally, a higher temperature than 25 °C enhances a passivation of the deposited lithium with electrolyte.[20,21]

All in all, thermal transients triggered different additional aging mechanisms compared to the steady-state reference cases and can thus not be considered for aging acceleration of steady-state lab conditions. However, they are relevant for application scenarios, where an interplay of charging and temperature transients can well occur[50] and could lead to significantly accelerated ageing compared to steady state lab conditions. This is in line with other investigations showing that, cells that were exposed to thermal transients have shown to go into thermal runaway even at mild temperatures.[17] Together, our findings underline the need to test more realistic temperature conditions also in the laboratory. In this context, the transferability of the results to other cell chemistries and geometries is of interest.

Research Article
doi.org/10.1002/batt.202300445
Chemistry Europe
European Chemical Societies Publishing

Experimental Section

The cells under investigation are high-energy 3.4 Ah pouch cells with tabs on the same side. Electrode sheets are wound. The voltage limits are specified by the manufacturer between 3 V and 4.35 V. The electrode material comprises of a graphite anode and a NMC532 cathode, which was measured via inductively coupled plasma optical emission spectroscopy (ICP) and scanning electron microscopy – energy dispersive X-ray spectroscopy (SEM-EDX). The cells were chosen because cells containing NMC532 can be regarded as state-of-the-art cathode material in automotive application.[51] NMC532 convinces with high thermal stability and capacity retention.[52]

The cells were cycled with a CTS Lab from BaSyTec GmbH. For mechanical and temperature control, they were clamped between aluminum plates with a constant pressure of 0.5 bar. The pressure was evenly distributed with bearings, springs and 1 mm silicon gap filler (TGF-V-Si, HALA Conec GmbH & Co. KG). This pressure was chosen because lower pressures have shown less cover layer formation and only slight inhomogeneities for pouch cells in comparison to higher pressures.[5] Similarly for prismatic cells, locally increasing stress was proposed to cause lithium plating.[53] With the chosen pressure in this investigation, any occurring inhomogeneities are most likely not due to pressure. Furthermore, the gap filler mitigated uneven surfaces and 0.5 mm thermocouples of type K (ES Electronic Sensor GmbH). The surface temperature was controlled with fluid channels in the aluminum plates. The fluid was supplied by three RE1050 S cryostats from LAUDA DR. R. WOBSER GMBH & CO. KG. The whole setup was placed inside a climate chamber that ensured a constant ambient temperature of 25 °C.

To enable fast temperature changes for the transient conditions, the fluid supply was controlled by pneumatic valves. An automatization routine in LabVIEW (National Instruments) controlled a relay that controls the valves. Two cells were cycled in pairs. An example for two cells cycled between 5 °C and 45 °C is given in Figure 6. At one point in time each cell was supplied by one cryostat, thus, had the according actual temperature T_{act}. As an example, one cell of the pair always had the temperature change from 45 °C to 5 °C at the beginning of charging, while the other cell had the temperature change from 5 °C to 45 °C respectively. This allowed for the specific investigation of the direction of the temperature change during charging. Reaching the final temperature at the surface of the cells took a couple of minutes. The entire charging process lasted about 1 h to 1.5 h at BoL depending on the temperature condition. During the temperature change in these first view minutes, bends in the voltage curves can be seen (Figure 7). We assume this to be mainly due to the temperature dependent resistances.[44] A drop in voltage during charging could also be attributed to lithium deposition as seen by Carter et al.[17] during a temperature change.

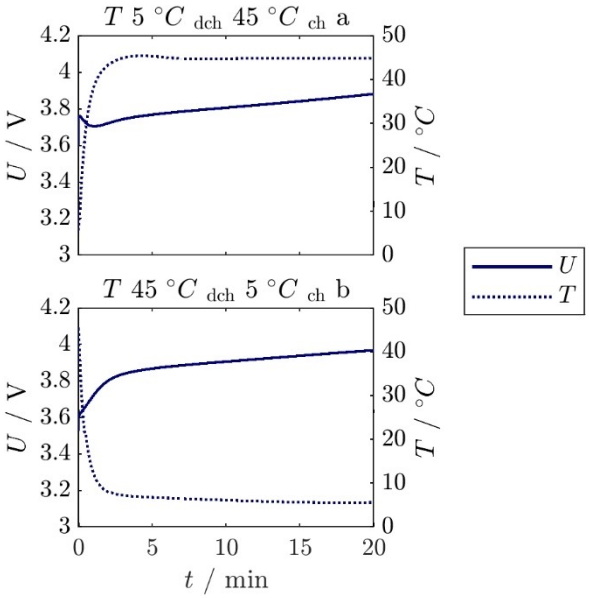

Figure 7. Voltage and surface temperature during temperature change from 5 °C to 45 °C (T 5 °C $_{dch}$ 45 °C $_{ch}$ *a*) and vice versa (T 45 °C $_{dch}$ 5 °C $_{ch}$ *b*) during charging.

Cycling Routine

Next to the cells, that experienced a superimposed temperature change during cycling, cells cycled at a constant temperature are considered as a reference scenario. Regarding the thermal boundary conditions, the first is considered transient and the second steady-state. The boundary condition does not reflect the temperature inside the cell. The spatial temperature field during load depends largely on the kind of the cooling condition.[54] For each steady-state condition (5 °C, 25 °C and 45 °C) at least two cells were cycled, indicated by "a" and "b" or "c". The temperature changes were performed for each combination of 5 °C, 25 °C and 45 °C. As an example, the actual mean surface temperatures during cycling are given for the reference cells (Table 2). These surface temperatures represent surface temperatures of the transient conditions according to T_{act}. The surface temperatures deviated slightly from the target temperature, because of heat losses and heat source during cycling. The constant charging rate was set to C/2 and the discharging rate to 1 C with a DoD of 70 % between the voltage limits of 3 V and 4.35 V.

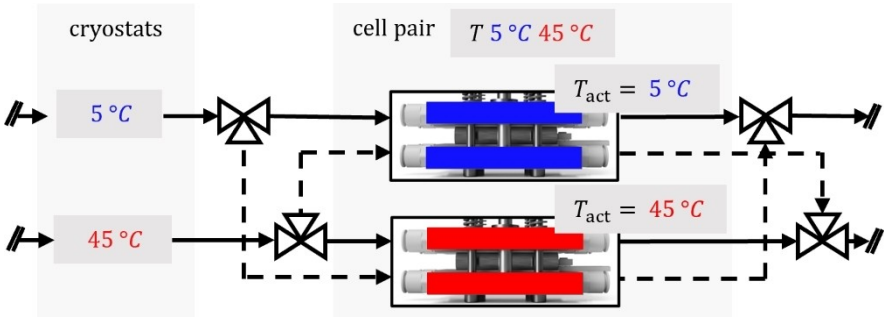

Figure 6. Schematic drawing of temperature change setup with the example for the cells cycled between 5 °C and 45 °C.

Table 2. Tested cells with measured mean surface temperatures during cycling.

Cell name	T / °C
5 °C *a*	6.24
25 °C *b*	25.15
45 °C *b*	45.07

Reference Performance Tests

The RPTs were performed in regular intervals every 100 to 150 full cycles depending on the cycling temperature. Lower temperatures lead to lower charge throughput as the cut-off voltages are reached due to higher overpotentials. To maintain similar time intervals for all cells, the cells cycled at lower temperatures performed more full cycles. For the RPT, the cryostats were set to 25 °C. The relaxation of the cells was controlled with the surface temperature probes. The RPT itself was designed to be as efficient as possible to suit the acceleration measurement. After a capacity measurement at the defined nominal C-rate, a quasi-OCV measurement in discharge and charge direction followed. Finally, an 18 s pulse measurement at 90 %, 50 % and 10 % SoC is conducted. The resistance of the pulses was evaluated after 18 s. The applied C-rates are listed in Table 3. The C-rate for the quasi-OCV was chosen as an optimum between testing time and informational content for DVA analysis.

The measured nominal capacity at BoL for all investigated cells is listed in Table 4. All cells exceed the nominal capacity of 3.4 Ah. Therefore, calendar aging previous to the cyclic aging tests conducted in this study is neglected. Furthermore, the coefficient of variation of this nominal capacity amounts to 0.70 %, which lies in the region of cell-to-cell variation due to manufacturing and supply summarized by Wildfeuer and Lienkamp.[55] In their literature study, they found the coefficient of variation to be in the region of 0.16 % to 2.36 %, while their latest study revealed low capacity coefficient of variation of 0.22 %.[55]

Table 3. RPT routine at 25 °C.

	C-rate/–
Nominal capacity	C/3
quasi-OCV	C/15
Pulse	1 C

Post-mortem Analysis

For the post-mortem analysis the cells were discharged with the defined C-rate of C/3 to the cut-off voltage. This means, that the cells all have an SoC of 0 % at their individual SoH. The cells were opened in a glove box under an inert argon atmosphere. The optical investigation was performed by scanning the cells in a flatbed scanner (Canon LiDE 300) or taking pictures with a camera (Olympus TG-6) immediately after the cell components were separated from each other.

In order to analyze the balancing of the investigated cell, pristine anode and cathode material were harvested and coin cells are built in half-cell configuration. The material was harvested under an inert argon atmosphere (O_2 concentration < 0.5 ppm, H_2O concentration < 0.5 ppm) in a glove box. Therefore, the respective material is initially decoated on one side, before electrode disc probes with 16 mm diameter are punched out. High-purity lithium metal discs with 16 mm diameter are used as counter electrode. Whatman GF/C separators, which are punched into 17 mm discs, are used as separators. The separator, which is 1 mm larger in diameter, is intended to prevent the anode and the cathode of the half-cell from making direct contact at the edge area. During assembling of the coin cells, the separator is soaked with 90 µL of LP57 electrolyte (1 M $LiPF_6$ in 3 : 7 EC/EMC). Additionally, a spring is embedded into the coin cell to assure even pressure and electrolyte distribution. The coin cells were cycled at room temperature using a Neware CT-4008T-5V10mA cycler. After an initial rest period of 24 hours, a formation cycle at C/3 is performed, followed by a low current quasi-OCV measurement at C/50 in both charge and discharge direction. The cut-off voltages were chosen between 3 V and 4.35 V for the cathode half-cell, respectively 0.005 V and 1.5 V for the anode half-cell.

Acknowledgements

L. C. and O. Q. gratefully acknowledge the financial support by Bundesministerium für Bildung und Forschung (BMBF 03XP0320D). A. C. gratefully acknowledges the financial support by Bundesministerium für Bildung und Forschung (BMBF 03XP0320A). The authors would like to thank Sabrina Herberger and Christof Pienkowski at KIT for their support. Additionally, the authors would like to thank Mark Junker and Gianluca Kox at RWTH for their support with the post mortem analysis. Open Access funding enabled and organized by Projekt DEAL.

Table 4. Measured nominal capacity (C/3) of all investigated cells at BoL.

Cell name	$C_{N(BoL)}$ / Ah	Cell name	$C_{N(BoL)}$ / Ah
5 °C *a*	3.504	***T* 5 °C$_{dch}$ 25 °C$_{ch}$ *a***	3.487
5 °C *b*	3.478	***T* 25 °C$_{dch}$ 5 °C$_{ch}$ *a***	3.497
5 °C *c*	3.480	***T* 25 °C$_{dch}$ 5 °C$_{ch}$ *b***	3.522
25 °C *a*	3.489	***T* 5 °C$_{dch}$ 45 °C$_{ch}$ *a***	3.450
25 °C *b*	3.443	***T* 45 °C$_{dch}$ 5 °C$_{ch}$ *a***	3.513
45 °C *a*	3.461	***T* 45 °C$_{dch}$ 5 °C$_{ch}$ *b***	3.446
45 °C *b*	3.486	***T* 25 °C$_{dch}$ 45 °C$_{ch}$ *a***	3.500
		T* 45 °C$_{dch}$ 25 °C$_{ch}$ *a	3.508

Conflict of Interests

The authors declare no conflict of interest.

Data Availability Statement

The data that support the findings of this study are available from the corresponding author upon reasonable request.

Keywords: lithium-ion battery · cyclic aging · thermal transient · aging acceleration · post-mortem analysis

[1] A. Barré, B. Deguilhem, S. Grolleau, M. Gérard, F. Suard, D. Riu, *J. Power Sources* **2013**, *241*, 680.
[2] D. Werner, S. Paarmann, A. Wiebelt, T. Wetzel, *Batteries* **2020**, *6*, 13.
[3] a) S. Gantenbein, M. Schönleber, M. Weiss, E. Ivers-Tiffée, *Sustainability* **2019**, *11*, 6697; b) J. Jiang, Y. Gao, C. Zhang, W. Zhang, Y. Jiang, *J. Electrochem. Soc.* **2019**, *166*, A1070–A1081.
[4] a) S. Watanabe, M. Kinoshita, T. Hosokawa, K. Morigaki, K. Nakura, *J. Power Sources* **2014**, *260*, 50; b) E. Wikner, E. Björklund, J. Fridner, D. Brandell, T. Thiringer, *Journal of Power Sources Advances* **2021**, *8*, 100054.
[5] D. Wasylowski, N. Kisseler, H. Ditler, M. Sonnet, G. Fuchs, F. Ringbeck, D. U. Sauer, *J. Power Sources* **2022**, *521*, 230825.
[6] S. Barcellona, L. Piegari, *J. Energy Storage* **2020**, *29*, 101310.
[7] W. Diao, S. Saxena, M. Pecht, *J. Power Sources* **2019**, *435*, 226830.
[8] K. Takei, K. Kumai, Y. Kobayashi, H. Miyashiro, N. Terada, T. Iwahori, T. Tanaka, *J. Power Sources* **2001**, *97(98)*, 697.
[9] a) W. Agyei Appiah, J. Park, S. Byun, Y. Roh, M.-H. Ryou, Y. M. Lee, *ChemElectroChem* **2019**, *6*, 3714; b) I. Bloom, B. Cole, J. Sohn, S. Jones, E. Polzin, V. Battaglia, G. Henriksen, C. Motloch, R. Richardson, T. Unkelhaeuser et al., *J. Power Sources* **2001**, *101*, 238.
[10] T. Gewald, M. Lienkamp, *Forsch. Ingenieurwes.* **2019**, *83*, 831.
[11] T. Waldmann, M. Wilka, M. Kasper, M. Fleischhammer, M. Wohlfahrt-Mehrens, *J. Power Sources* **2014**, *262*, 129.
[12] D. Werner, S. Paarmann, A. Wiebelt, T. Wetzel, *Batteries* **2020**, *6*, 12.
[13] A. Tourani, P. White, P. Ivey, *J. Power Sources* **2014**, *268*, 301.
[14] S. S. Zhang, K. Xu, T. R. Jow, *J. Power Sources* **2004**, *130*, 281.
[15] P. Ramadass, B. Haran, R. White, B. N. Popov, *J. Power Sources* **2002**, *112*, 606.
[16] S. Paarmann, K. Schuld, T. Wetzel, *Energy Tech* **2022**, *10*, 2200384.
[17] R. Carter, E. J. Klein, T. A. Kingston, C. T. Love, *Front. Energy Res.* **2019**, *7*, 144.
[18] P. Arora, M. Doyle, R. E. White, *J. Electrochem. Soc.* **1999**, *146*, 3543.
[19] R. Imhof, P. Novák, *J. Electrochem. Soc.* **1998**, *145*, 1081.
[20] Q. Q. Liu, D. J. Xiong, R. Petibon, C. Y. Du, J. R. Dahn, *J. Electrochem. Soc.* **2016**, *163*, A3010–A3015.
[21] W. Chang, C. Bommier, T. Fair, J. Yeung, S. Patil, D. Steingart, *J. Electrochem. Soc. Interface* **2020**, *167*, 90503.
[22] V. Ruiz, A. Kriston, I. Adanouj, M. Destro, D. Fontana, A. Pfrang, *Electrochim. Acta* **2017**, *240*, 495.
[23] M. Lewerenz, A. Warnecke, D. U. Sauer, *J. Power Sources* **2017**, *354*, 157.
[24] I. Bloom, A. N. Jansen, D. P. Abraham, J. Knuth, S. A. Jones, V. S. Battaglia, G. L. Henriksen, *J. Power Sources* **2004**, *139*, 295.
[25] M. Steinhauer, S. Risse, N. Wagner, K. A. Friedrich, *Electrochim. Acta* **2017**, *228*, 652.
[26] K. Xu, A. von Cresce, U. Lee, *Langmuir: the ACS journal of surfaces and colloids* **2010**, *26*, 11538.
[27] D. Zhang, B. Haran, A. Durairajan, R. White, Y. Podrazhansky, B. Popov, *J. Power Sources* **2000**, *91*, 122.
[28] M. Lewerenz, C. Rahe, G. Fuchs, C. Endisch, D. U. Sauer, *J. Energy Storage* **2020**, *30*, 101529.
[29] L. Willenberg, P. Dechent, G. Fuchs, M. Teuber, M. Eckert, M. Graff, N. Kürten, D. U. Sauer, E. Figgemeier, *J. Electrochem. Soc.* **2020**, *167*, 120502.
[30] M. Dubarry, B. Y. Liaw, *J. Power Sources* **2009**, *194*, 541.
[31] J. A. Gilbert, I. A. Shkrob, D. P. Abraham, *J. Electrochem. Soc.* **2017**, *164*, A389–A399.
[32] M. Lewerenz, A. Marongiu, A. Warnecke, D. U. Sauer, *J. Power Sources* **2017**, *368*, 57.
[33] M. Lewerenz, A. Warnecke, D. U. Sauer, *J. Power Sources* **2017**, *369*, 122.
[34] M. Ecker, P. Shafiei Sabet, D. U. Sauer, *Appl. Energy* **2017**, *206*, 934.
[35] H. Lin, D. Chua, M. Salomon, H.-C. Shiao, M. Hendrickson, E. Plichta, S. Slane, *Electrochem. Solid-State Lett.* **2001**, *4*, A71.
[36] J. C. Burns, D. A. Stevens, J. R. Dahn, *J. Electrochem. Soc.* **2015**, *162*, A959–A964.
[37] M. Tang, P. Albertus, J. Newman, *J. Electrochem. Soc.* **2009**, *156*, A390.
[38] F. Grimsmann, T. Gerbert, F. Brauchle, A. Gruhle, J. Parisi, M. Knipper, *J. Energy Storage* **2018**, *15*, 17.
[39] S. J. Harris, A. Timmons, D. R. Baker, C. Monroe, *Chem. Phys. Lett.* **2010**, *485*, 265.
[40] P. M. Attia, A. Bills, F. Brosa Planella, P. Dechent, G. dos Reis, M. Dubarry, P. Gasper, R. Gilchrist, S. Greenbank, D. Howey et al., *J. Electrochem. Soc.* **2022**, *169*, 60517.
[41] O. Queisser, L. Cloos, F. Boehm, D. Oehler, T. Wetzel, *Energy Technol.* **2021**, *9*, 2000915.
[42] D. Andre, M. Meiler, K. Steiner, C. Wimmer, T. Soczka-Guth, D. U. Sauer, *J. Power Sources* **2011**, *196*, 5334.
[43] D. R. Ely, R. E. García, *J. Electrochem. Soc.* **2013**, *160*, A662–A668.
[44] D. Andre, M. Meiler, K. Steiner, H. Walz, T. Soczka-Guth, D. U. Sauer, *J. Power Sources* **2011**, *196*, 5349.
[45] S. Paarmann, L. Cloos, J. Technau, T. Wetzel, *Energy Technol.* **2021**, *9*, 2000862.
[46] M. Klett, R. Eriksson, J. Groot, P. Svens, K. Ciosek Högström, R. W. Lindström, H. Berg, T. Gustafson, G. Lindbergh, K. Edström, *J. Power Sources* **2014**, *257*, 126.
[47] M. Storch, J. P. Fath, J. Sieg, D. Vrankovic, C. Krupp, B. Spier, R. Riedel, *J. Energy Storage* **2021**, *41*, 102887.
[48] T. Waldmann, B.-I. Hogg, M. Kasper, S. Grolleau, C. G. Couceiro, K. Trad, B. P. Matadi, M. Wohlfahrt-Mehrens, *J. Electrochem. Soc.* **2016**, *163*, A1232–A1238.
[49] C. Fear, M. Parmananda, V. Kabra, R. Carter, C. T. Love, P. P. Mukherjee, *Energy Storage Mater.* **2021**, *35*, 500.
[50] S. Goutam, A. Nikolian, J. Jaguemont, J. Smekens, N. Omar, P. van Dan Bossche, J. van Mierlo, *Appl. Therm. Eng.* **2017**, *126*, 796.
[51] R. Schmuch, R. Wagner, G. Hörpel, T. Placke, M. Winter, *Nat. Energy* **2018**, *3*, 267.
[52] H.-J. Noh, S. Youn, C. S. Yoon, Y.-K. Sun, *J. Power Sources* **2013**, *233*, 121.
[53] A. J. Smith, Y. Fang, A. Mikheenkova, H. Ekström, P. Svens, I. Ahmed, M. J. Lacey, G. Lindbergh, I. Furó, R. W. Lindström, *J. Power Sources* **2023**, *573*, 233118.
[54] Z. Li, J. Zhang, B. Wu, J. Huang, Z. Nie, Y. Sun, F. An, N. Wu, *J. Power Sources* **2013**, *241*, 536.
[55] L. Wildfeuer, M. Lienkamp, *eTransportation* **2021**, *9*, 100129.

Manuscript received: October 2, 2023
Revised manuscript received: December 8, 2023
Accepted manuscript online: December 12, 2023
Version of record online: December 21, 2023